Available online at www.sciencedirect.com
ScienceDirect
International Journal of Pharmaceutics 343 (2007) 173–180
INTERNATIONAL JOURNAL OF PHARMACEUTICS
www.elsevier.com/locate/ijpharm

Application of molecular modelling to determine the surface energy of mannitol

A. Saxena [a], J. Kendrick [b], I. Grimsey [a,*], L. Mackin [c]

[a] *Drug Delivery Group, Institute of Pharmaceutical Innovation, School of Pharmacy, University of Bradford, Bradford, UK*
[b] *The Computational Group, Institute of Pharmaceutical Innovation, School of Pharmacy, University of Bradford, Bradford, UK*
[c] *Product Development, Pharmaceutical & Analytical R&D, AstraZeneca, Macclesfield, UK*

Received 20 December 2006; received in revised form 10 May 2007; accepted 12 May 2007
Available online 18 May 2007

Abstract

In this paper, molecular modelling was used to investigate the nature of probe/surface interactions during the analysis of Dβ-mannitol using inverse gas chromatography (IGC). IGC was used to experimentally measure the dispersive components of surface free energy (γ_S^D) and the specific components of free energy of adsorption ($-\Delta G_A^{SP}$) of Dβ-mannitol by calculating the retention time of non-polar (*n*-alkanes) and polar (tetrahydrofuran and chloroform) probes, respectively. The results showed that Dβ-mannitol surface is acidic in nature because the basic probe had more interaction with the surface as compared to acidic probe. Cerius^2 software package was used to model the two morphologically important surfaces, which showed the presence of surface hydroxyl groups. Molecular dynamics simulations were performed in Cerius^2 to model the adsorption of the same probes (*n*-alkanes, tetrahydrofuran and chloroform) on the Dβ-mannitol surfaces. The adsorption energies calculated from the simulation showed a close match to those determined experimentally. The calculated values are slightly higher for all probes except chloroform, but as a single perfect crystal was modelled without considering the effect of impurities, solvent and other physical factors this is not unexpected.

Keywords: Inverse gas chromatography; Surface free energy; Mannitol; Crystal surface; Molecular modelling

1. Introduction

The surface energetics of pharmaceutical solids has been reported to influence a number of processes which occur during pharmaceutical processing and formulation. These processes include solid–liquid and solid–solid contact. The examples of solid–liquid contact are wet granulation (Buckton, 1992), suspension formulation (Young and Buckton, 1990; Parsons et al., 1992), dissolution (Lippold and Ohm, 1986) and film coating (Rowe, 1988). Whereas powder mixing and flow (Staniforth, 1985; Ahfat et al., 1997), and drug interaction with the container (Traini et al., 2006) involve solid–solid contact. A number of techniques have been employed to measure the surface energetics of pharmaceutical systems. However, all the techniques utilised have some limitations in their methodology (Buckton et al., 1995).

From Ticehurst et al. (1994) to Swaminathan et al. (2006) there are a good number of research papers explaining the use of inverse gas chromatography (IGC) to analyse the surface properties and the changes in surface energetic of various pharmaceutical powders. In IGC, the sample is packed into a column and its surface properties are analysed by measuring the retention behaviour of known vapour probes. These probes, which are injected at infinite dilution, are selected to target acidic, basic and dispersive interactions with the crystal surface (Ticehurst et al., 1994).

The experimental measurement of surface energetic parameters of pharmaceutical crystals is routine, but the use of molecular modelling approaches to understand the nature of interactions between the probes (adsorbate) and the surfaces (adsorbent), at the molecular level have been limited. Molecular modelling provides knowledge of orientation and exposure of molecular groups on pharmaceutical (Grimsey et al., 1999; York et al., 1998) and non-pharmaceutical surfaces (Oliver et al., 1997; Dekkers et al., 2001). This technique has also been employed to simulate the adsorption of small molecules on the

* Corresponding author. Tel.: +44 1274 234754; fax: +44 1274 234769.
E-mail address: i.m.grimsey@bradford.ac.uk (I. Grimsey).

0378-5173/$ – see front matter © 2007 Elsevier B.V. All rights reserved.
doi:10.1016/j.ijpharm.2007.05.019

surfaces of non-pharmaceutical crystals (Pradip, 2002, 2003; Pradip et al., 2002; Gocmez, 2006; Xu, 2006). The simulated results have been compared with the experimental data on non-pharmaceutical materials obtained from inverse gas chromatography (Allington et al., 1998, 2004).

For pharmaceutical materials, molecular modelling has been used to calculate a potential grid around an isolated molecule of adsorbent. Surface adsorption was then modelled to evaluate the interaction energies between individual atoms of adsorbate molecule and atoms of the adsorbent molecule oriented as if they were in the surface (Grimsey et al., 2002). The main limitation of this published work was that the single molecule of adsorbent was considered as the representative of the whole surface and all atoms of this molecule are accessible by the approaching molecule of adsorbate. Whereas, when the adsorbent molecule is present on the surface then only the atoms or functional groups exposed on the surface are able to interact. The rest of the molecule is not free to interact because of stearic hindrance or intermolecular bonding.

In this paper two of the most important morphological surfaces of Dβ-mannitol crystals were modelled and different probes were allowed to interact with the surfaces using molecular dynamic calculations which allowed the calculation of the adsorption energy of the probe on these surfaces. The results of these calculations are then compared with the experimental results for the adsorption of these probes on the crystal surfaces using inverse gas chromatography.

2. Materials and methods

2.1. Materials

Dβ-Mannitol B.P. (>98% pure), which is a common pharmaceutical excipient, was supplied by Roquette UK limited. IGC probes (HPLC grade) were hexane (BDH Chemicals), heptane (Sigma–Aldrich), octane (Aldrich), nonane (Aldrich), tetrahydrofuran, (Riedel-deHaen) and chloroform (Fisher).

2.2. Methods

2.2.1. Inverse gas chromatography

Full details of the experimental procedure of inverse gas chromatography have been published previously by Ticehurst et al. (1994). Two pre-silanised columns of dimensions, 2 m (three loops) × 6 mm (outer diameter) × 4 mm (inner diameter), were packed with Dβ-mannitol and each column was analysed twice at room temperature of 30 °C and zero relative humidity, using dry nitrogen gas as the carrier. The retention time (t_r) of a series of *n*-alkanes (non-polar probes, hexane to nonane) and polar probes (THF and chloroform) were measured and converted to the retention volume (V_n) using:

$$V_n = (t_r - t_d)Fj \quad (1)$$

where F is the carrier flow-rate, t_d is the retention time of non-interacting gas and j is the gas compressibility factor.

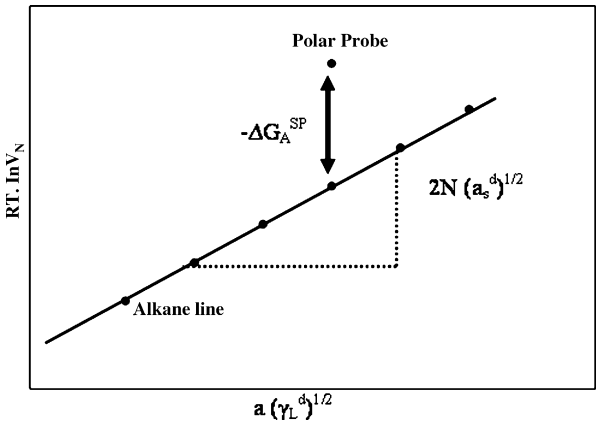

Fig. 1. Schematic diagram showing the determination of the dispersive and specific components of the surface free energy of adsorption.

The dispersive component of the surface free energy (γ_S^D) and the specific component of the free energy of adsorption ($-\Delta G_A^{SP}$) were determined by the method of Schultz and Lavielle (1989). The dispersive component of surface free energy (γ_S^D) was calculated using a series of *n*-alkanes (Fig. 1) using Eq. (2).

$$RT \ln V_n = a(\gamma_L^D)^{1/2} 2N(\gamma_S^D)^{1/2} + C \quad (2)$$

where N is Avogadro's number, a is the probe interaction surface area, γ_L^D is the surface tension of the probe and R is the gas constant.

The specific component of the free energy of adsorption is calculated by plotting the retention volume (V_n) of the polar probes on the same graph. These data points will lie above the line formed by the alkane probes and $-\Delta G_A^{SP}$ is given by the deviation of each point from the alkane line (Fig. 1).

2.2.2. Molecular modelling

Seven different crystal structures of mannitol were obtained from the Cambridge Structural Database (Cambridge Crystallographic Data Centre, Cambridge, UK, CSD version 5.27, November 2005) using ConQuest version 1.8. A summary of the structures, space group and polymorph is given in Table 2. The structures were used to develop and validate the force-field which was used for further calculations of the adsorption energetics.

2.2.2.1. Calculation of point charges. A single, isolated molecule of mannitol was extracted from each of these crystal structures and was optimised using the General Atomic and Molecular Electronic Structure System-UK (GAMESS) molecular orbital package. *Ab initio* molecular orbital calculations were performed at Hartree-Fock 6-31G* level to calculate the electrostatic potential around the geometry optimised molecule. Point charges were derived from the electrostatic potential around the molecule using a least square fit of the potential from the charges to the *ab initio* calculated potential (Kendrick and Fox, 1991). The electrostatic potential of the probe molecules was calculated in a similar way, but instead of using the exper-

imental crystal structure as a starting point for the geometry optimisation, the lowest energy conformation of each probe molecule was determined by energy minimisation.

2.2.2.2. Force-field. Molecular mechanics calculations using the DREIDING II force-field (Mayo et al., 1990) were performed to optimise the crystal structure, both the lattice parameters and the molecular coordinates. By default the force-field as implemented in Cerius^2 uses settings which are more appropriate for gas or solution phase simulation, rather than the present solid state simulation, so the suitability of these defaults settings was explored by comparing the predicted, calculated lattice parameters of the seven experimental structures. By default the Dreiding force-field uses:

- A Lennard-Jones 12-6 potential for van der Waals interaction;
- An atom-based summation for coulomb and van der Waals interaction with a cut-off;
- A distance-dependent dielectric constant;
- A specific functional representation of hydrogen bonding.

The use of the real space cut-offs is not appropriate for the molecules which have long range electrostatic interaction. Therefore, the use of the Ewald method was investigated, which is able to calculate the electrostatic energy accurately (to within a specified numerical precision) and has better convergence properties.

The distance-dependent dielectric constant is mainly used for the liquid simulations to model the "screening" by solvent molecules. As a part the evaluation of the force-field the effect of removing distance dependency in the dielectric constant was examined. The electrostatic contribution to hydrogen bonding is significant and as a result it also decided to examine the effect of removing the specific hydrogen bonding term that the default Dreiding force-field uses. Finally the use of a Buckingham potential (or exponential-6) potential to describe the van der Waals interactions in place of the default Lennard Jones potential was also examined.

2.2.2.3. Modelling of crystal surface. Out of seven different structures, the beta form of mannitol having lowest *R* factor (experimentally analysed at room temperature, CSD reference code DMANTL07) was selected (Table 1). The *R* factor measures the precision of a structure determination, a lower *R* factor indicates a smaller difference between the observed data and the calculated model. This particular form of mannitol was selected because it was the Dβ-mannitol, which was analysed by inverse gas chromatography at room temperature. Cerius^2 (Molecular Simulations Inc., San Diego, CA, USA) was used to apply Bravais–Freidel–Donnay–Harker (BFDH) method to predict the crystal morphology. The BFDH method is a geometrical calculation that uses the crystal lattice and symmetry to generate a list of possible growth faces and their relative growth rates. The approach is based solely on the interplanar spacing, d_{hkl}, of the different crystal faces, with the lowest growth rates occurring at the faces with the greatest d_{hkl}. So the faces with the slowest growth rates and largest surface area are the most morphologically important (Coombes et al., 2002). The molecular arrangement of these surfaces was generated in Cerius^2.

2.2.2.4. Molecular dynamics. Cerius^2 was used to perform a molecular dynamics simulation of the probe molecules on the surface of mannitol. The surface was represented by a slab whose thickness was large enough so that the energy of lower surface should not affect the energy of upper surface. The slab was minimised (relaxed) and the molecules in the slab were then kept fixed during the molecular dynamics (MD) simulation. NVE molecular dynamics simulations (a system of a fixed number of particles (*N*), in a fixed volume (*V*), and with a fixed total energy (*E*)) were performed for 50 ps with an integration step of 1 fs. The initial temperature of the simulation was 300 K. Equilibration was determined by examination of the change in average potential energy as a function of time. A number of structures were randomly selected from the trajectory after equilibration and minimised. The average minimised energy was used as the energy of the system. The energy of the isolated probe molecules was calculated in the same way. The adsorption energy E_{ads} is then defined as

$$E_{system} = E_{probe} + E_{surface} - E_{ads} \quad (3)$$

where E_{system} = average minimised energy of the system (probe/surface interaction); E_{probe} = average minimised energy of isolated probe; $E_{surface}$ = average minimised energy of surface (the energy of the surface is taken to be zero as the surface was fixed during simulation).

Table 1
Details of seven different mannitol structures obtained from Cambridge Structural Database

CSD reference code	Space group	Polymorph	*R*-factor (%)	Measurement temperature	Authors/journal
DMANTL	$P2_12_12_1$	Dβ	18.0	RT	Berman et al. (1968)
DMANTL01	$P2_12_12_1$	Dκ	4.9	RT	Kim et al. (1968)
DMANTL07	$P2_12_12_1$	Dβ	2.8	RT	Kaminsky and Glazer (1997)
DMANTL08	$P2_12_12_1$	Dα	5.4	100K	Fronczek et al. (2003)
DMANTL09	$P2_12_12_1$	Dβ	3.6	100K	Fronczek et al. (2003)
DMANTL10	$P2_1$	Dδ	3.1	100K	Fronczek et al. (2003)
DLMANT	$Pna2_1$	DL	3.0	123K	Kanters et al. (1977)

RT = room temperature.

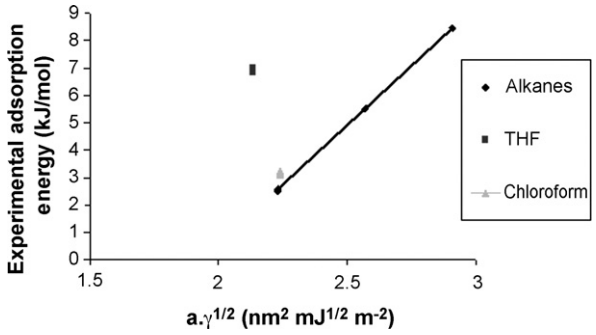

Fig. 2. The experimental adsorption energy of different probes on Dβ-mannitol measured by inverse gas chromatography.

3. Results and discussion

3.1. Inverse gas chromatography

Fig. 2 shows that tetrahydrofuran (THF), which a basic probe has high net retention volume (V_n) on Dβ-mannitol as compared to chloroform (an acidic probe). This reflects the acidic nature of the Dβ-mannitol surface.

The acidic sites on mannitol are believed to be the exposed oxygen atoms whilst the dispersive sites are presumed to be the exposed carbon atoms in the chain (Grimsey et al., 1999).

3.2. Molecular modelling

3.2.1. Force-field

Several parameters of the force-field, including the form of the potentials and some of the values for the terms in the potential, were modified in a systematic fashion so that the energy minimised crystal structures reproduced the available experimental structures as well as possible. After examination of several force-fields the following modifications were made:

- An exponential-6 potential was used for the van der Waals interaction;
- The Ewald method was used for coulombs interactions;
- A distance independent dielectric constant was used;
- No specific hydrogen bonding term was used.

Table 2 shows that the default Dreiding force-field predicts significantly larger deviations from experiment than the modified force-field. It was also found the default force-field to be very sensitive to the values of the cut-off parameter for the van der Waals and electrostatic interactions. The modified force-field shows reasonable predictions of all of the crystal lattice parameters, with the largest deviation (4.6%) occurring for the lattice parameter of DMANTL01. Because of the ability of the modified force-field to represent all of the different crystal structures it was selected for the further study of adsorption on to the surface of mannitol.

3.2.2. Crystal morphology

Fig. 3 shows the crystal morphology predicted by Cerius[2] using the BFDH method.

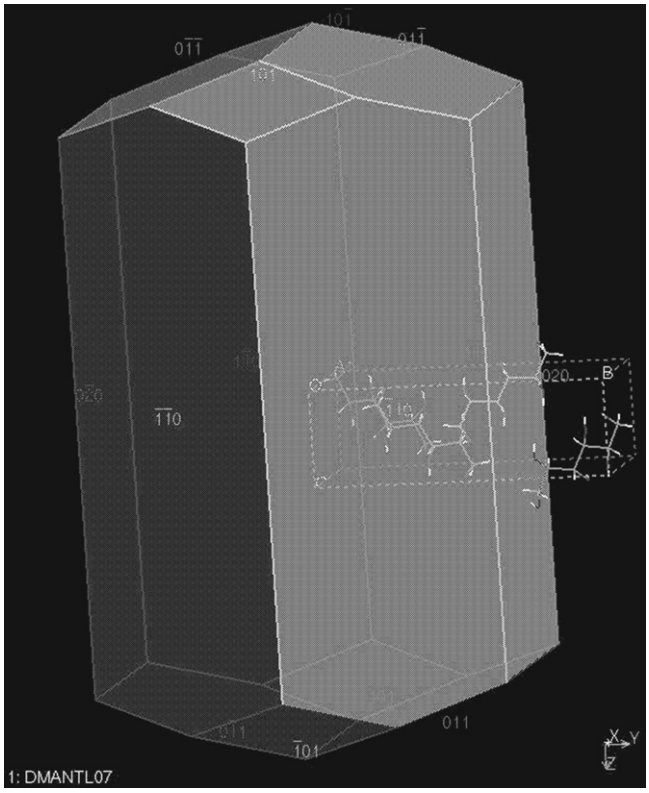

Fig. 3. Morphological prediction of mannitol crystal faces.

The predicted crystal morphology was similar to the morphology observed under the microscope (Figs. 3 and 4). In the predicted morphology the (0 2 0) face has highest percentage area 13.7%, whereas (1 $\bar{1}$ 0) face has 11.7% area. As the material is being milled, it is assumed that the particles will preferentially split along the preferred cleavage plane, which has been

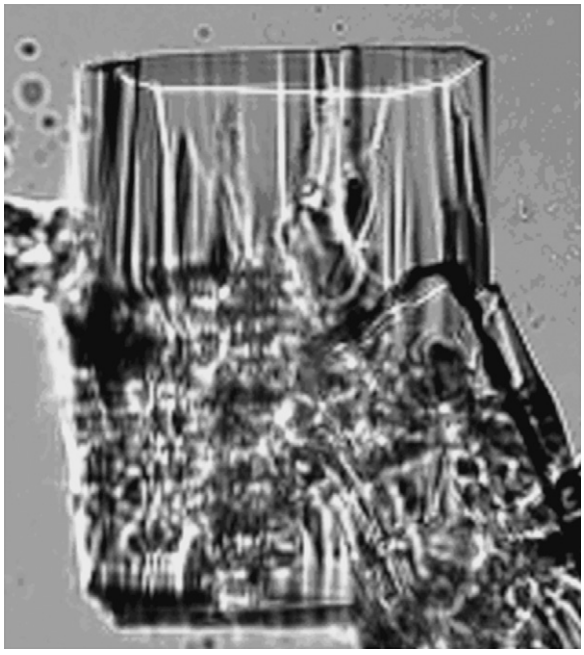

Fig. 4. Crystal morphology of mannitol under microscope.

Table 2
Comparison between experimental and minimised lattice parameters by applying the default Dreiding and modified force-field

CSD reference code	Experimental lattice parameter (Å)	Default force-field		Modified force-field	
		Minimised lattice parameters (Å)	%Diff	Minimised lattice parameters (Å)	%Diff
DMANTL					
a	9.048	8.455	−6.6	8.703	−3.8
b	4.870	5.178	6.3	4.883	0.3
c	18.262	18.373	0.6	18.737	2.6
DLMANT					
a	8.672	8.500	−2.0	8.485	−2.2
b	16.875	16.749	−0.7	16.361	−3.0
c	5.560	5.673	2.0	5.663	1.9
DMANTL01					
a	8.942	8.878	−0.7	8.528	−4.6
b	18.798	18.319	−2.5	18.642	−0.8
c	4.893	4.930	0.8	4.955	1.3
DMANTL07					
a	8.694	8.868	2.0	8.474	−2.5
b	16.902	16.412	−2.9	16.479	−2.5
c	5.549	5.578	0.5	5.659	2.0
DMANTL08					
a	4.865	4.888	0.5	4.964	2.0
b	8.873	8.827	−0.5	8.518	−4.0
c	18.739	18.808	0.4	18.635	−0.6
DMANTL09					
a	5.538	5.573	0.6	5.659	2.2
b	8.580	8.452	−1.5	8.468	−1.3
c	16.795	16.701	−0.6	16.474	−1.9
DMANTL10					
a	4.899	5.324	8.7	5.006	2.2
b	18.268	18.252	−0.1	18.346	0.4
c	5.043	4.963	−1.6	4.935	−2.1

a, *b* and *c* are lattice parameters of crystal structure. %diff = percentage difference between experimental and minimised lattice parameters.

assumed to be the crystal face with highest surface area. In Dβ-mannitol whose space group is $P2_12_12_1$, (0 2 0) is equivalent to (0 $\bar{2}$ 0) and (1 $\bar{1}$ 0) is equivalent to (1 1 0), ($\bar{1}$ $\bar{1}$ 0) and ($\bar{1}$ 1 0) due to screw axis. This means that (0 2 0), (1 $\bar{1}$ 0) and their equivalent faces will cover around 75% of the total crystal surface. So the molecular arrangement of these two faces has significant influence on the surface energy of the whole crystal. These two faces were visualised by slicing through the bulk structure along the required hkl plane.

3.2.3. Molecular arrangement of mannitol faces

Figs. 5 and 6 show the molecular arrangement of relaxed (0 2 0) and (1 $\bar{1}$ 0) faces, respectively, which indicates the presence of hydroxyl (–OH) groups on both surfaces. So the region of high acidity of mannitol crystal as per IGC results can be related to the presence of these acidic hydroxyl (–OH) on the surface.

3.2.4. Molecular dynamics

In molecular dynamics simulations the (0 2 0) and (1 $\bar{1}$ 0) surfaces were represented by a six unit cell thick slab. These slabs were relaxed and the molecules in the slab were then kept fixed during MD simulation. Molecular dynamics simulations of probe molecules on the (0 2 0) and (1 $\bar{1}$ 0) slabs were performed within the NVE ensemble. The average temperature over the equilibrated trajectories was around 300 K. Fig. 7 shows the behaviour of the average potential energy as a function of time. The equilibration time is taken to be the time it takes for the average potential energy to reach a constant value.

The average minimised energy of randomly selected structures (15–25 structures) after the equilibration time was used to calculate the energy of the system. In the same way energy of the isolated probe was calculated but without the mannitol surface. The adsorption energies for *n*-alkanes and polar probes on (0 2 0) and (1 $\bar{1}$ 0) faces were calculated using Eq. (3) and summarised in Tables 3 and 4, respectively.

The graph between adsorption energy and root square of area and surface tension of vapour probes ($a\gamma^{1/2}$) (Table 1) were plotted for (0 2 0) and (1 $\bar{1}$ 0) faces (Figs. 8 and 9) using the same approach as for the experimental determination of the surface energies by IGC.

3.2.5. Comparison of inverse gas chromatography and molecular modelling results

The dispersive component of the surface free energy (γ_S^D) and the specific component of the free energy of adsorption

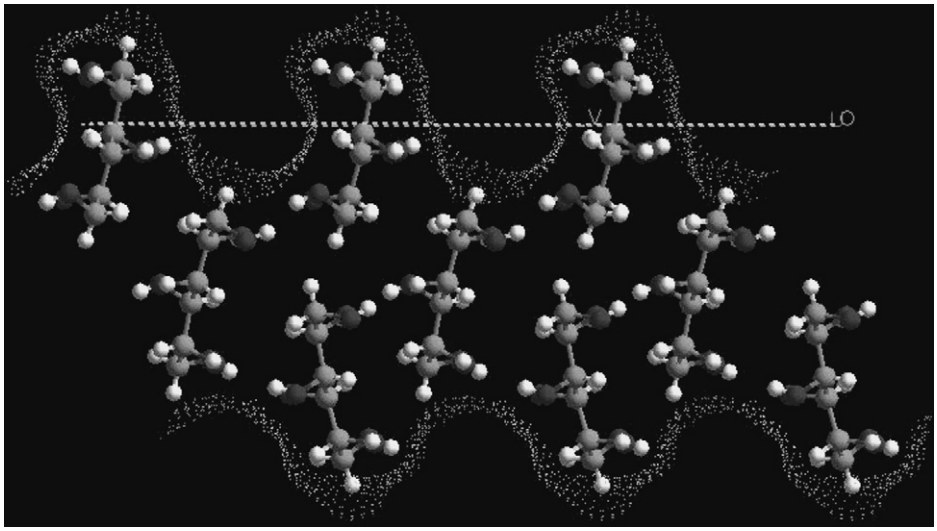

Fig. 5. Molecular arrangement of the (0 2 0) face of mannitol.

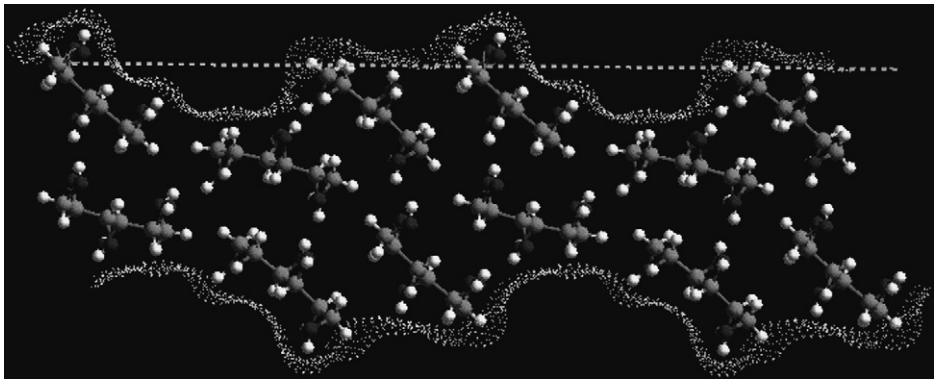

Fig. 6. Molecular arrangement of the (1 $\bar{1}$ 0) face of mannitol.

Table 3
The calculated adsorption energy of probes on the (0 2 0) face of Dβ-mannitol

Probes	Average energy of probe (kJ/mol)	Average energy of probe on surface (kJ/mol)	Adsorption energy (kJ/mol)	$a\gamma^{1/2}$ ($nm^2\ mJ^{1/2}\ m^{-2}$)
n-Alkane				
Hexane	4.9	−41.8	46.7	2.2306
Heptane	72.0	22.1	49.9	2.5682
Octane	30.3	−22.6	52.9	2.9076
Polar probe				
THF	35.0	−15.9	50.9	2.1345
Chloroform	0.0	−47.2	47.2	2.2392

Table 4
The calculated adsorption energy of probes on the (1 $\bar{1}$ 0) face of Dβ-mannitol.

Probes	Average energy of probe (kJ/mol)	Average energy of probe on surface (kJ/mol)	Adsorption energy (kJ/mol)	$a\gamma^{1/2}$ ($nm^2\ mJ^{1/2}\ m^{-2}$)
n-Alkane				
Hexane	4.9	-36.2	41.2	2.2306
Heptane	72.0	27.6	44.4	2.5682
Octane	30.3	-17.0	47.3	2.9076
Polar probe				
THF	35.0	-10.5	45.6	2.1345
Chloroform	0.0	-41.1	41.1	2.2392

Table 5
Comparison of dispersive energy and specific component of free energy calculated by IGC and molecular modelling.

Method	Face	γ_S^D (mJ m^{-2})	$-\Delta G_A^{SP}$ (kJ/mol)	
			THF	Chloroform
Inverse gas chromatography		48.2 (±0.68)	4.7 (±0.35)	0.5 (±0.12)
Molecular modelling	(0 2 0)	56.2	5.0	0.3
	(1 $\bar{1}$ 0)	55.3	5.1	−0.2

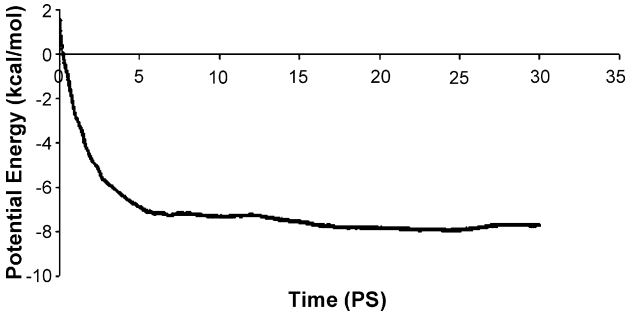

Fig. 7. The running average of potential energy (kcal/mol) during a molecular dynamics simulation.

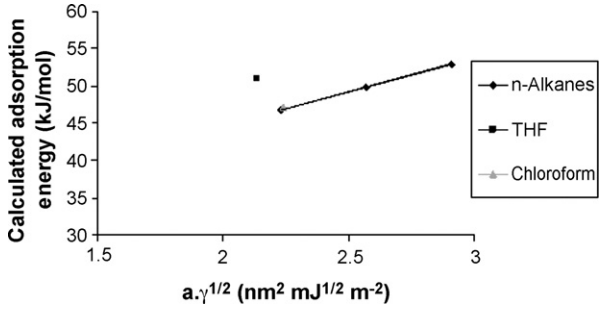

Fig. 8. Figure showing the calculated adsorption energy of different probes on the (0 2 0) face.

($-\Delta G_A^{SP}$) for the probes on the Dβ-mannitol were calculated from IGC (Fig. 2) and molecular modelling of (0 2 0) and (1 $\bar{1}$ 0) faces of Dβ-mannitol (Figs. 8 and 9, respectively). The dispersive component of the surface free energy (γ_S^D) was calculated from the slope of the *n*-alkanes line whereas the specific components of the free energy of adsorption ($-\Delta G_A^{SP}$) for polar probes were calculated from their distance from the *n*-alkanes straight line (Fig. 1). Table 5 summarises both the IGC and molecular modelling results. This shows that modelling gave a higher value for both the dispersive interaction with the alkanes and specific interactions for THF whilst the values for chloroform were marginally lower. There are three proposed reasons for this difference. First is that a single perfect crystal was modelled without considering the effect of impurities, solvent and other physical factors. The second reason is that during the simulation, the mannitol surface was fixed, which allows the best possible interaction of single molecule of probe on the surface. Third, the effect of temperature during MD simulations was not taken into account. The comparison between the modelling results on two different faces showed the interactions between the dispersive interaction for alkane probes as well as specific interaction for THF were essentially similar. Modelling of chloroform indicates that (0 2 0) face does show a higher interaction as compared to (1 $\bar{1}$ 0) but in both cases this interaction is small reflecting the essentially acidic nature of mannitol and the difference could be classed as insignificant in comparison to the variance of the experimentally measured values.

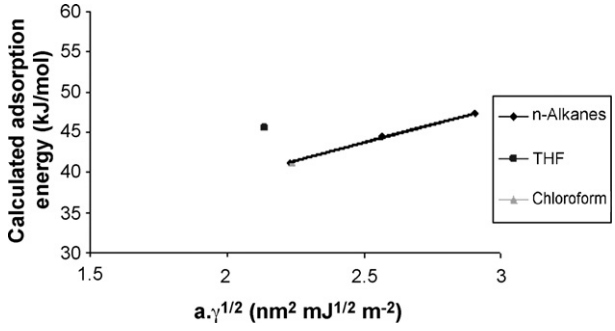

Fig. 9. Figure showing the calculated adsorption energy of different probes on (1 $\bar{1}$ 0) face.

4. Conclusion

This paper showed that molecular modelling technique can be used to calculate surface energetic values of a solid material that are essentially the same as those measured under experimental conditions. IGC results showed higher interaction of THF with mannitol as compared to chloroform, indicating that mannitol is acidic in nature. This was supported by molecular modelling by predicting a high density of hydroxyl groups on the mannitol surface. This shows that the application of molecular modelling has given valuable knowledge about the interaction mechanisms underlying the measured values. With this example, it is clear that by combining both experimental and computational techniques, an insight can be gained into the nature of interactions with the surface of pharmaceutical materials and the possibility of being able to predict experimental values based on theoretical calculations.

Acknowledgements

We acknowledge AstraZeneca and University of Bradford for a studentship for A. Saxena in support of this work.

References

Ahfat, N.M., Buckton, G., Burrows, R., Ticehurst, M.D., 1997. Predicting mixing performance using surface energy measurements. Int. J. Pharm. 156, 89–95.

Allington, R.D., Attwood, D., Hamerton, I., Hay, J.N., Howlin, B.J., 1998. A model of the surface of oxidatively treated carbon fibre based on calculations of adsorption interactions with small molecules. Composites: Part A 29A, 1283–1290.

Allington, R.D., Attwood, D., Hamerton, I., Hay, J.N., Howlin, B.J., 2004. Developing improved models of oxidatively treated carbon fibre surfaces, using molecular simulation. Composites: Part A 35, 1161–1173.

Berman, H.M., Jeffrey, G.A., Rosentein, R.D., 1968. The crystal structures of the R' and B forms of D-Mannitol. Acta. Crystallogr. B24, 442–449.

Buckton, G., 1992. The estimation and application of surface energy data for powdered systems. Drug Dev. Ind. Pharm. 18, 1149–1167.

Buckton, G., Darcy, P., Mccarthy, D.M., 1995. The extent of errors associated with contact angles.3. The influence of surface-roughness effects on angles measured using a Wilhelmy plate technique for powders. Colloid. Surf. A. 95, 27–35.

Coombes, D.S., Catlow, C.R.A., Gale, J.D., Hardy, M.J., Saunders, M.R., 2002. Theoretical and experimental investigations on the morphology and pharmaceutical crystals. J. Pharm. Sci. 91, 1652–1658.

Dekkers, R., Woensdregt, C.F., Wollants, P., 2001. Surface modelling of crystalline non-metallic inclusions. J. Non-Crystalline Solids 282, 49–60.

Fronczek, F.R., Kamel, H.N., Slattery, M., 2003. Three polymorphs (alpha, beta and delta) of D-Mannitol at 100 K. Acta Crystallogr. C 59, 567–570.

Gocmez, H., 2006. The interaction of organic dispersant with alumina: a molecular modelling approach. Ceram. Int. 32, 521–525.

Grimsey, I.M., Sunkersett, M., Osborn, J.C., York, P., Rowe, R.C., 1999. Interpretation of the differences in the surface energetics of two optical forms of mannitol by inverse gas chromatography and molecular modelling. Int. J. Pharm. 191, 43–50.

Grimsey, I.M., Osborn, J.C., Doughty, S.W., York, P., Rowe, R.C., 2002. The application of molecular modelling to the interpretation of inverse gas chromatography data. J. Chromatogr. A 969, 49–57.

Kaminsky, W., Glazer, A.M., 1997. Crystal optics of D-Mannitol, $C_6H_{14}O_6$: crystal growth, structure, basic physical properties, birefringence, optical activity, Faraday effect, electro-optic effects and model calculations. Zeitschrift Fur Kristallographie 212, 283–296.

Kanters, J.A., Roelofsen, G., Smits, D., 1977. Crystal and molecular-structure of D-L-Mannitol at −150 °C. Acta Crystallogr. B 33, 3635–3640.

Kendrick, J., Fox, M., 1991. Calculation and display of electrostatic potentials. J. Mol. Graphics 9, 182–187.

Kim, H.S., Jeffrey, G.A., Rosenstein, R.D., 1968. The crystal structure of the K form of D-Mannitol. Acta Cryst. B24, 1449–1455.

Lippold, B.C., Ohm, A., 1986. Correlation Between wettability and dissolution rate of pharmaceutical powders. Int. J. Pharm. 28, 67–74.

Mayo, S.L., Olafson, B.D., Goddard, W.A., 1990. Dreiding—a generic force-field for molecular simulations. J. Phys. Chem. 94, 8897–8909.

Oliver, P.M., Watson, G.W., Kelsey, E.T., Parker, S.C., 1997. Atomistic simulation of the surface structure of the TiO_2 polymorphs rutile and anatase. J. Mater. Chem. 7, 563–568.

Parsons, G.E., Buckton, G., Chatham, S.M., 1992. The use of surface energy and polarity determinations to predict physical stability of non-polar, non-aqueous suspensions. Int. J. Pharm. 83, 163–170.

Pradip, R.B., 2002. Design of tailor-made surfactants for industrial applications using a molecular modelling approach. Colloids Surf. A: Physicochem. Eng. Aspects 205, 139–148.

Pradip, R.B., Rao, T.K., Krishnamurthy, S., Vetrivel, R., Mielczarski, J., Cases, J.M., 2002. Molecular modelling of interactions of alkyl hydroxamates with calcium minerals. J. Colloids Interface Sci. 256, 106–113.

Pradip, R.B., 2003. Molecular modelling and rational design of flotation reagents. Int. J. Mineral Process. 72, 95–110.

Rowe, R.C., 1988. Adhesion of film coatings to tablet surfaces – a theoretical approach based on solubility parameters. Int. J. Pharm. 41, 219–222.

Schultz, J., Lavielle, L., 1989. Interfacial properties of carbon-fiber epoxy matrix composites. In: Acs Symposium Series, pp. 391185–391202.

Staniforth, J.N., 1985. Ordered mixing or spontaneous granulation. Powder Technol. 45, 73–77.

Swaminathan, V., Cobb, J., Saracovan, I., 2006. Measurement of the Surface energy of lubricated pharmaceutical powders by inverse gas chromatography. Int. J. Pharm. 312, 158–165.

Ticehurst, M.D., Rowe, R.C., York, P., 1994. Determination of the surface-properties of 2 batches of salbutamol sulfate by inverse gas-chromatography. Int. J. Pharm. 111, 241–249.

Traini, D., Young, P.M., Rogueda, P., Price, R., 2006. The use of AFM and surface energy measurement to investigate drug-canister material interactions in a model pressurized dose inhaler formulation. Aerosol Sci. Technol. 40, 227–236.

Xu, J., 2006. Molecular dynamics modelling of adsorption of hedp on calcite surface. Acta Phys. Sinica 55, 1107–1112.

York, P., Ticehurst, M.D., Osborn, J.C., Roberts, R.J., Rowe, R.C., 1998. Characterisation of the surface energetics of milled dl-propranolol hydrochloride using inverse gas chromatography and molecular modelling. Int. J. Pharm. 174, 179–186.

Young, S.A., Buckton, G., 1990. Particle growth in aqueous suspensions—the influence of surface-energy and polarity. Int. J. Pharm. 60, 235–241.